

Cloud patterns have four interpretable dimensions

Martin Janssens¹, Jordi Vilà-Guerau de Arellano¹, Marten Scheffer¹, Coco Antonissen², A. Pier Siebesma^{2,3}, Franziska Glassmeier²

¹Wageningen University & Research

²Delft University of Technology

³Royal Netherlands Meteorological Institute

Key Points:

- Shallow cloud field patterns in satellite observations are quantified by 21 metrics and follow a unimodal, continuous distribution.
- Most existing metrics are redundant; 4 principal components capture 82% of the variance of 21 metrics.
- Characteristic length, void size, directional alignment and cloud-top height variance combine to effectively describe the patterns.

Corresponding author: Martin Janssens, martin.janssens@wur.nl

14 Abstract

15 Shallow cloud fields over the subtropical ocean exhibit many spatial patterns. The frequency
 16 of occurrence of these patterns can change under global warming. Hence, they may influence
 17 subtropical marine clouds' climate feedback. While numerous metrics have been proposed
 18 to quantify cloud patterns, a systematic, widely accepted description is still missing. There-
 19 fore, this paper suggests one. We compute 21 metrics for 5000 satellite scenes of shallow
 20 clouds over the subtropical Atlantic Ocean and translate the resulting dataset to its prin-
 21 cipal components (PCs). This yields a unimodal, continuous distribution without distinct
 22 classes, whose first four PCs explain 82% of all 21 metrics' variance. The PCs correspond
 23 to four interpretable dimensions: *Characteristic length*, *void size*, *directional alignment* and
 24 horizontal *cloud-top height variance*. These dimensions span a space in which an effective
 25 pattern description can be given, which may be used to better understand the patterns'
 26 underlying physics and feedback on climate.

27 Plain Language Summary

28 Satellite images show that clouds which develop in the lowest five kilometres of the
 29 atmosphere organise into many visually distinct patterns. Because different patterns have
 30 different radiative properties, a change in the relative occurrence of a pattern may influence
 31 Earth's response to warming. To study this effect, the patterns must first be quantified;
 32 numerous metrics have been developed for this task. In this paper, we compute 21 such
 33 metrics for 5000 cloud fields observed by satellite over the Atlantic Ocean east of Barbados.
 34 We show that the information contained in the 21 metrics can already very accurately be
 35 described by only 4 derived metrics, which capture a cloud field's typical cloud size, the size
 36 of connected clear sky patches, the clouds' degree of directional alignment and variance in
 37 cloud-top height. Combinations of these 4 metrics do not identify the existence of typical
 38 patterns, as previously suggested. However, they form a new, effective and interpretable
 39 pattern description, which can be used to better understand how cloud fields organise and
 40 how this impacts the wider climate system.

41 1 Introduction

42 Shallow cumulus clouds are the most abundant cloud type over the tropical oceans
 43 (Johnson et al., 1999), but result from many interacting processes and scales. This combi-
 44 nation makes them the most uncertain aspect of how clouds will feed back onto a warming
 45 climate (e.g. Bony & Dufresne, 2005; Schneider et al., 2017). Several mechanisms that gov-
 46 ern this response have recently been uncovered (Rieck et al., 2012; Bretherton, 2015; Klein
 47 et al., 2017). However, the origins and sensitivity of the rich spectrum of spatial patterns ex-
 48 hibited by shallow cloud fields has remained rather unexplored (Nuijens & Siebesma, 2019).
 49 Such spatial patterns alter precipitation distributions in cloud resolving simulations of deep
 50 convection in warmer conditions (Muller & Held, 2012; Tobin et al., 2012); recent research
 51 indicates that spatial patterning may influence the low cloud climate feedback too (Bony et
 52 al., 2020). Establishing this contribution of shallow cloud-field patterns and its underlying
 53 physics are therefore important research objectives.

54 The first step of such research is to classify or quantitatively measure any characteristic
 55 of the horizontal dimension of a shallow cloud field. Two comprehensive, complementing
 56 approaches were recently proposed: Expert visual inspection, which returns subjective, but
 57 interpretable classes of patterns (Stevens et al., 2019) and unsupervised machine learn-
 58 ing, which is challenging to interpret, but gives more objectively inferred pattern measures
 59 (Denby, 2020). A third, more traditional approach is to compute one or more human-
 60 defined metrics; these are both interpretable and objective and are therefore considered in
 61 this paper.

Quantified patterns are often associated with a quantity called “organisation”. This term has consequently taken on numerous interpretations. It is often synonymous with “aggregation” in studies of deep convection (Tobin et al., 2012; White et al., 2018; Holloway et al., 2017), sometimes characterised as the regular, random or clustered structure of nearest neighbour distances of cloud objects (Weger et al., 1992; Seifert & Heus, 2013; Tompkins & Semie, 2017), or connected to cloud scale (Neggers et al., 2019; Bony et al., 2020). However, cloud field organisation has also been defined by metrics of fractal analysis (Cahalan & Joseph, 1989), directional alignment (Brune et al., 2018), subcritical percolation (Windmiller, 2017) or spatial variance (de Roode et al., 2004; Wood & Hartmann, 2006). While this makes it difficult to objectively define and discuss organisation, all these interpretations share the same aim: Quantifying cloud field patterns. Hence, this diversity can potentially also be harnessed to distinguish between different patterns.

The aim of this paper is therefore to systematically extract the independent information encapsulated by the set of metrics associated with “cloud field organisation” in literature, and to use this information to describe and interpret cloud field patterns as effectively as possible. We first compute 21 diverse metrics for 5000 satellite observations of mesoscale cloud fields in the trades and synthesise these in a multivariate distribution (section 2). Next, we show that these metrics vary primarily along 4 principal components, allowing drastic dimensionality reduction (section 3.1). Analysis of these main principal components results in a pattern description that is remarkably effective, in addition to being interpretable and objective (section 3.2). We then highlight several approaches to approximate the principal components that balance the description’s complexity and accuracy (section 3.3). Finally, we demonstrate and discuss the ability of our description to characterise previously diagnosed and novel regimes of characteristic patterns (section 3.4), before concluding (section 4).

2 Constructing a cloud field pattern distribution

2.1 Data

Following Stevens et al. (2019) and Bony et al. (2020), we concentrate on shallow, subtropical clouds in the marine North Atlantic trades east of Barbados (20°-30°N, 48°-58°W), which are representative for the entire trades (Medeiros & Nuijens, 2016). Our cloud fields stem from the MODIS instrument borne by NASA’s Aqua and Terra satellites. Specifically, we sample daytime overpasses during December-May 2002-2020 and directly use the level 2 Cloud Water Path (CWP), Cloud-Top Height (CTH) and cloud mask products at 1km resolution (Platnick et al., 2015) as basis for our metrics. Fig. S1 shows that the results are not overly sensitive to resolution. We only interpret pixels classified as “confidently cloudy” by the cloud mask algorithm as cloud.

Our data points are scenes of cloud fields, which are 512km×512km subsets sampled within the 10°×10° observation region. To boost the size of our dataset, scenes are allowed to overlap 256km. We attempt to minimise the impact of errors and biases in remotely sensed cloud products by rejecting scenes with i) high clouds such as cirrus wisps, if more than 20% of the clouds’ tops lie above 5km, ii) overly large sensor zenith angle, if this angle exceeds 45°, following e.g. Wood and Field (2011) and iii) sunglint errors, manually excluding scenes where these are visually found to influence the cloud mask. A set of 5004 scenes remains.

2.2 Metrics and dimensionality reduction

To appropriately capture the body of existing organisation metrics, we require them to meet either of the following two criteria: i) Are they perceived to capture a unique aspect of the patterns? or ii) do they frequently recur or recently first appear in literature? Additionally, they must be easy to interpret. This procedure (see tab. S1 for details) diagnoses 21 metrics, which broadly divide into three categories: Statistical moments of

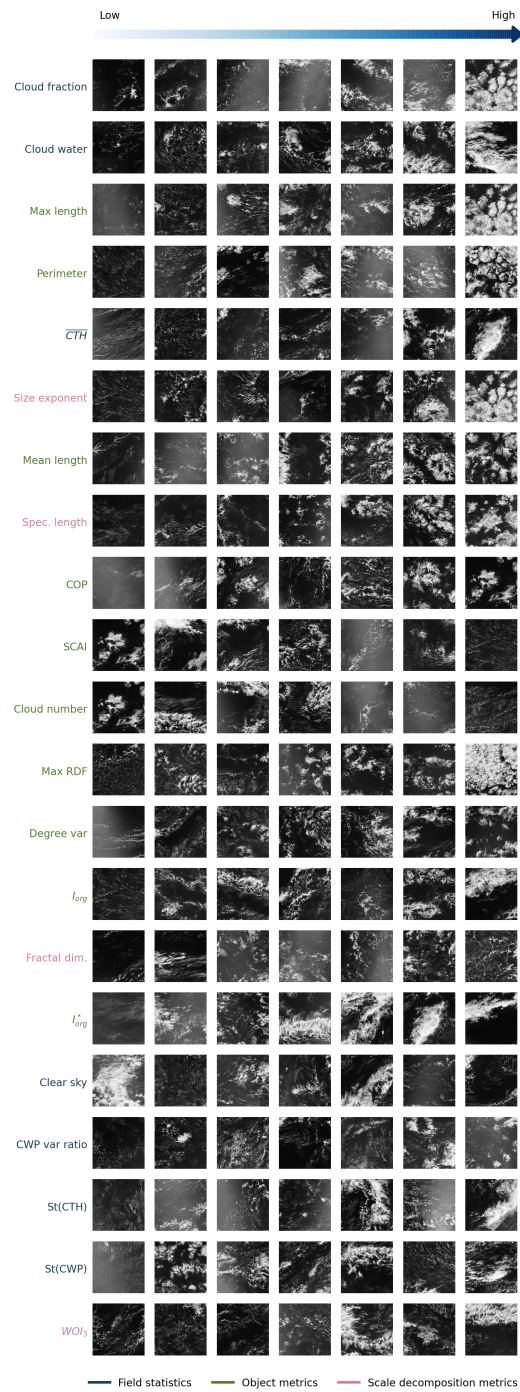


Figure 1. Visual representation of scenes ordered by metrics derived from three categories (text colour) and sampled at linear intervals. Bright backgrounds stem from sunglint, which is accounted for in metric computations.

111 physical cloud field properties, object-based metrics, and attributes of scale decompositions.
 112 These metrics are briefly introduced below, visually presented in fig. 1 and further detailed
 113 in Text S1.

114 Statistical moments of cloud field properties comprise measures of typical cloud mass
 115 and area: The cloud mask’s coverage fraction (Cloud fraction), the CWP’s scene integral
 116 (Cloud water) and standard deviation (St(CWP)) and the variance ratio for “mesoscale
 117 aggregation” of moisture proposed by Bretherton and Blossey (2017) (CWP var. ratio),
 118 here applied only to cloud water. Furthermore, this class contains measures of the clouds’
 119 vertical extent: The mean and standard deviation of cloud-top height ($\overline{\text{CTH}}$ and St(CTH)
 120 respectively).

121 Object-based metrics measure size, shape and relative positioning of individual cloud
 122 segments, which are identified from cloud mask fields using 4-connectivity labelling. To
 123 avoid artefacts at the resolution scale, objects of a smaller dimension than four times the
 124 instrument resolution are ignored. Our results are not sensitive to the chosen connectivity
 125 scheme or minimum object size (see fig. S1). The resulting metrics further divide into
 126 two categories: Scene statistics of individual object properties and measures of the spa-
 127 tial distribution of the objects. The first category includes the mean and maximum object
 128 length (Mean length, Max length), the number of objects (Cloud number) and the mean ob-
 129 ject perimeter (Perimeter); the second comprises the Simple Convective Aggregation Index
 130 (SCAI) (Tobin et al., 2012), Convective Organisation Potential (COP) (White et al., 2018),
 131 the peak of the average radial distribution function (Rasp et al., 2018) (Max RDF), the
 132 degree variance (Degree var) of the cloud objects’ nearest-neighbour network representation
 133 (Glassmeier & Feingold, 2017) and the Organisation Index (I_{org}) (Weger et al., 1992), of
 134 which we include two versions. The first, most commonly applied form, compares the cloud
 135 field nearest-neighbour cumulative density function (NNCDF) to a Weibull distribution.
 136 The second variant (I_{org}^*) compares it to an inhibition NNCDF that accounts for object size
 137 and therefore is less likely to erroneously predict regularity in the cloud fields (Benner &
 138 Curry, 1998). This metric is similar to that introduced by Pscheidt et al. (2019).

139 We compute four metrics from scale decompositions: The size exponent of the cloud
 140 object size distribution modelled as a power law (Size exponent), the box-counting dimension
 141 of cloud boundaries in the cloud mask field (Fractal dim.), the Spectral length scale as defined
 142 by Jonker et al. (1999) and the deviation of variance from the mean in the horizontal, vertical
 143 or diagonal orientations of the cloud water field’s stationary wavelet spectrum (WOI_3)
 144 (Brune et al., 2018). In this paper, we use these metrics as discriminators between individual
 145 cloud fields, not to measure their cumulative scaling properties. Finally, we introduce a novel
 146 metric: A scene’s largest, rectangular, contiguous cloud-free area (Clear sky), as a simple
 147 measure of *lacunarity*, the degree to which continuous areas without clouds dominate a
 148 scene.

149 We describe patterns as a linear combination of the computed metrics, which are stan-
 150 dardised to weight them equally. Since many metrics in fig. 1 strongly correlate (see fig.
 151 S2), they are treated to a Principal Component Analysis (PCA, e.g. Abdi and Williams
 152 (2010)). This transforms the metrics to an orthogonal basis whose components (principal
 153 components - PCs) explain the maximum variance in the dataset. If a *small* number of
 154 PCs (orthogonal dimensions) can accurately capture the metric set’s variance, these form
 155 an effective pattern description.

156 3 Describing patterns

157 3.1 A four-dimensional pattern distribution

158 Figure 2 shows uni- and bivariate kernel density estimates on planes spanned by the
 159 first four PCs of the metric distribution, annotated with the fractional variance of the
 160 dataset explained by each PC (explained variance ratio - EVR). It reveals that multiple

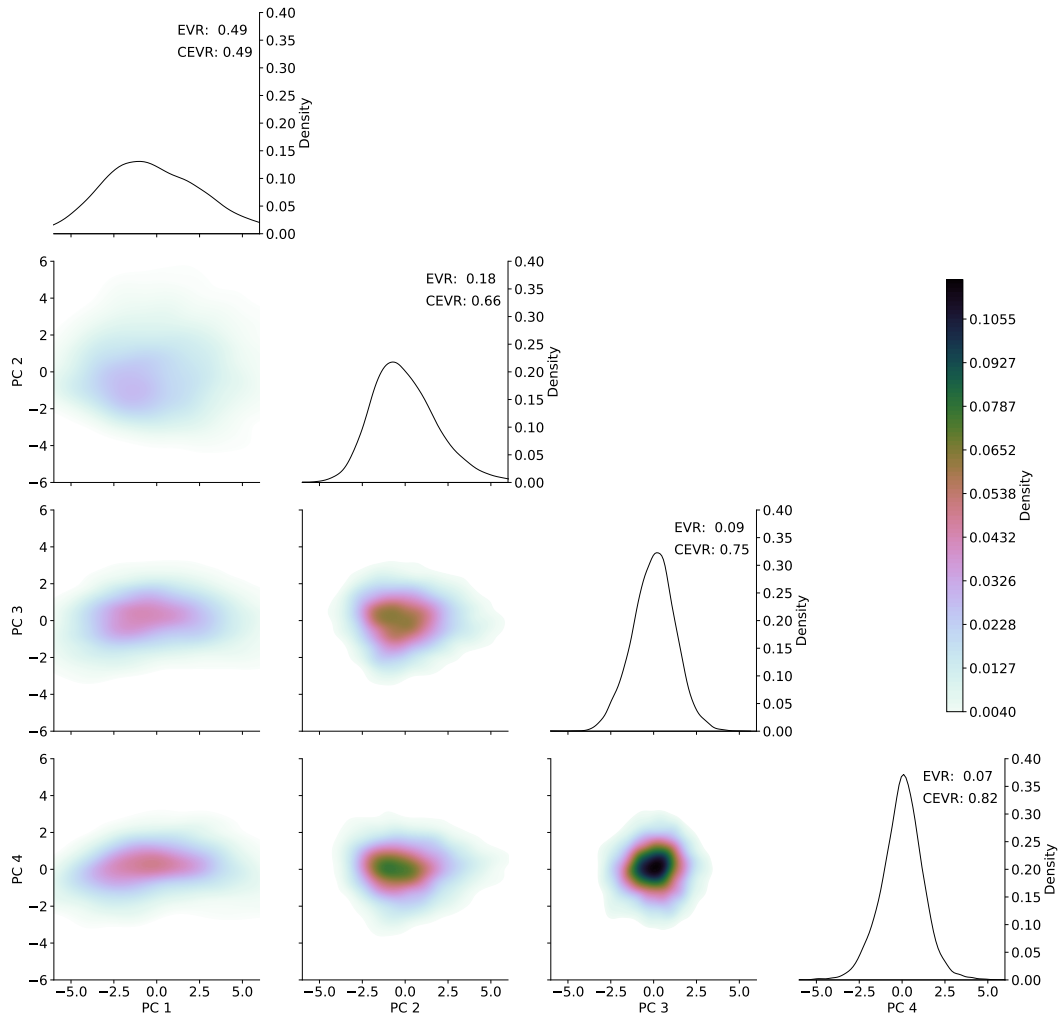


Figure 2. Univariate (diagonal, density on y-axis) and bivariate (off-diagonal, density in colour) Gaussian kernel density estimates of the first four principal components (PCs) of the pattern distribution. The annotations EVR and CEVR denote the individual and cumulative explained variance ratio of each PC, respectively. Bandwidths for the Gaussian kernels are computed using Scott's rule (Scott, 1992).

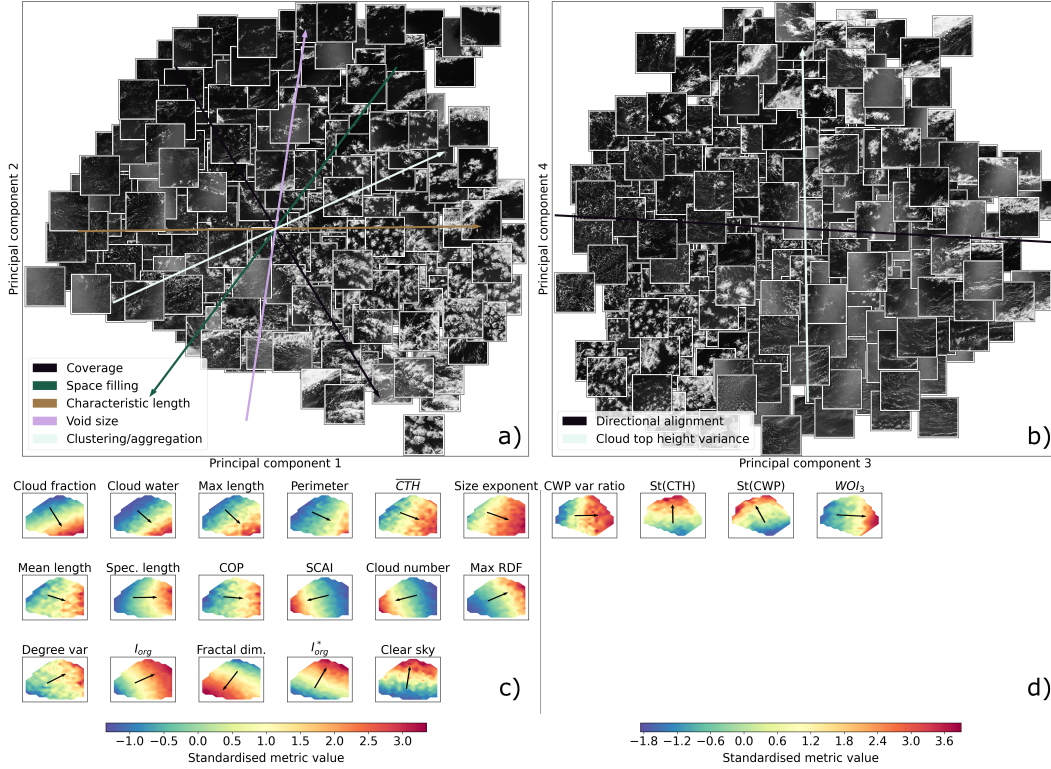


Figure 3. Top: Images of scenes projected onto planes spanned by the first and second (a) and third and fourth (b) PCs of the metric distribution, overlaid by arrows oriented along the mean gradient of several metric groups (see main text). Bottom: Filled contours of standardised metric values that have in excess of 50% of their variance explained by the first (c) and second (d) plane, constructed by piecewise linear barycentric interpolation and overlaid by an arrow pointing along the mean gradient. Subfigures b) and d) are rotated counter-clockwise by 49° in-plane to improve clarity of visualisation.

161 PCs (dimensions) are needed to capture the multivariate distribution’s cumulative EVR
 162 (CEVR) appropriately. However, the first PC is by far the most influential (EVR=0.49 -
 163 widest distribution). Furthermore, the CEVR of the first two PCs already rises to 0.66,
 164 while including 3 and 4 of the 21 original dimensions explains 75% and 82% of the dataset’s
 165 variance, respectively. After the fourth PC, EVR quickly deflates (PCs 5-9 have EVRs
 166 of 0.04, 0.03, 0.03, 0.02, 0.02), dropping below 0.01 after the tenth PC (fig. S3). These
 167 statistics show that four PCs effectively capture the information in all 21 metrics. Therefore,
 168 we reduce our 21-dimensional metric set to these four PCs.

169 Of course, truncating the PCA after precisely four components remains somewhat ar-
 170 bitrary. Yet, this choice strikes a useful balance between including enough dimensions to
 171 effectively describe patterns and sufficiently few dimensions to interpret them. This claim
 172 is visually supported by fig. 3 a) and b) (fig. S3 adds quantitative evidence): Combinations
 173 of PC1 and PC2 (fig. 3 a) consistently and coherently position visually similar (different)
 174 scenes close to (far from) each other. PC3 and PC4 (fig. 3 b) ably reveal further distinctions.
 175 Hence, linear combinations of these four PCs form an effective pattern description.

3.2 An interpretable pattern description

Our four-dimensional pattern description is not only effective; by relating the PCs to their underpinning metrics, it can also be interpreted. This interpretation is facilitated by fig. 3 c) and d), which show the in-plane gradient and mean direction of change of metrics that predominantly vary in the planes depicted in fig. 3 a) and b) respectively. By averaging the gradients of several similarly varying metrics, we identify a meaningful vocabulary that labels several directions of change in the two planes (arrows in fig. 3 a and b). Using this vocabulary, we name the principal components and relate them to several common interpretations of organisation.

Strikingly, 17/21 metrics mainly describe variations in the first two PCs (fig. 3 c, see also fig. S4). These metrics derive from all three categories (field statistics, objects and scale decompositions) and point in a rather continuous spectrum of directions, offering a remarkable number of interesting choices for interpreting fig. 3 a):

1. *Coverage* (Arrow in fig. 3 a represents the mean gradient of Cloud fraction, Max length and Cloud water)
2. *Space filling* (Fractal dim., I_{org}^*)
3. *Characteristic length* (Spectral length scale, Size exponent, Mean length)
4. *Void size* (Clear sky)
5. *Aggregation or clustering* (I_{org} , SCAI, Cloud number, Max RDF), as commonly associated with deep convective organisation (Tompkins & Semie, 2017; Tobin et al., 2012).

We adopt the two directions that best align themselves with the PCs as names for our pattern description’s first two dimensions: *Characteristic length* and *void size*. We find it both intuitive and beautiful that these two dimensions, which respectively measure the typical scale of clouds and the complementary clear sky space between them, naturally emerge from our approach.

Linear combinations of the PCs can construct different terms in the quintet above. For instance, *clustering/aggregation* differs only subtly from *characteristic length*, assigning slightly more importance to voids between cloud clusters. *Space filling* weights voids even more heavily. Finally, *coverage* distinguishes itself from *void size* by assigning marginally more importance to characteristic length. Hence, the same aspects of the patterns in fig. 3 a) can be described with different pairs of terms.

Several such pairs are already indirectly recognised as central traits of “organisation”. For instance, Seifert and Heus (2013) suggest that both a spectral length scale (*characteristic length*) and I_{org} (*clustering*) may be needed to discriminate between various modes of organisation; Neggers et al. (2019) identify organisation as a combination of maximum cloud size (*coverage*) and typical nearest-neighbour distances between smaller clouds (*space filling*); chapter 5 of van Laar (2019) distinguishes “cloud field characteristics” (cloud fraction, maximum cloud size - *coverage*) from “organisation parameters” (I_{org} , SCAI, COP - *clustering*) and Bony et al. (2020) span their planar description of organisation with mean length (*characteristic length*) and I_{org} (*clustering*). The arrows in Figure 3 relate all these interpretations to each other.

However, our four-dimensional pattern description goes beyond these common, two-dimensional interpretations of organisation. Figure 3 d) shows that the third and fourth PC distinguish patterns with different directional alignment (WOI_3) of the scene’s larger scales (CWP var ratio) and those with different horizontal variance of vertical cloud development (St(CTH)). Hence, variations in PC 3 and PC4 can be understood as combinations of *directional alignment* and *cloud-top height variance*.

224 Summarising, we propose to think of cloud field patterns, as described by organisation
 225 metrics, as a linear combination of the 4 PCs: *Characteristic length*, *void size*, *directional*
 226 *alignment* and *cloud-top height variance*, each term contributing a dimension that is un-
 227 correlated to the others. However, many valid interpretations exist, especially of the first
 228 two dimensions. Therefore, the consistency with which “organisation” is understood can
 229 be considerably advanced by using the relationships between the various interpretations
 230 established in this section.

231 3.3 Selecting metric subsets

232 While four PCs describe patterns remarkably well, they still require input from *all*
 233 metrics. If added interpretability or less computation is desired, one might approximate
 234 the PCs with a subset of metrics. This approach challenges each chosen metric to do
 235 considerably more work than merely inspiring an interpretation of the PCs, as in the previous
 236 section, since no metric subset is fully orthogonal or optimally variance-capturing. Moreover,
 237 it is often not obvious that a given metric is much better suited to approximate a PC than
 238 a similarly varying one. This problem is illustrated by applying *sparse* PCA (Zou et al.,
 239 2006) to our data. Despite optimising a cost function that explicitly balances the accuracy
 240 of the approximate PCs with how many metrics contribute to them, this technique cannot
 241 robustly indicate metric subsets (see fig. S5).

242 One practical way to compose a subset nonetheless is choosing one metric that most
 243 closely correlates to each PC (Cadima & Jolliffe, 1995). This approach selects the Spectral
 244 length scale, Clear sky, WOI_3 and St(CTH) (CEVR=0.59) and is a reasonable approxi-
 245 mation of the PC description (CEVR=0.82). If one’s primary interest is in the first two
 246 dimensions of the pattern distribution, several roughly orthogonal metric pairs competently
 247 estimate the plane in fig. 3 a). Examples include Spectral slope and Clear sky (CEVR=0.31),
 248 Cloud fraction and Fractal dim. (CEVR=0.31) or Perimeter and I_{org}^* (CEVR=0.30). All
 249 three pairs sacrifice explained variance compared to two PCs (CEVR=0.66). Yet, they cap-
 250 ture far more information than various metric combinations considered in literature, e.g.
 251 Cloud number and I_{org} (Bony et al., 2020, CEVR=0.18), I_{org} and Fractal dim. (Denby,
 252 2020, CEVR=0.20), Spec. Length and I_{org} (Seifert & Heus, 2013, CEVR=0.19) or I_{org} ,
 253 SCAI, COP and Max RDF (van Laar, 2019, CEVR=0.26). Therefore, we recommend to
 254 always assess the orthogonality and EVR of one’s metrics with a PCA, before optionally
 255 selecting a metric subset that approximates their desirable properties appropriately.

256 3.4 Regimes of patterns

257 Asking how many dimensions cloud field patterns possess is not equal to asking how
 258 many fundamental types of cloud patterns exist. Dividing clouds into distinct classes (e.g.
 259 cumulus or cirrus) is a classical approach, which recently inspired efforts to also classify
 260 shallow cloud field patterns, using both the human eye (Stevens et al., 2019) and metrics
 261 (Bony et al., 2020). We compare our pattern description to these classes (“sugar”, “gravel”,
 262 “fish” and “flowers”) by identifying seven k-means clusters in the four-dimensional PC
 263 distribution (fig. 4).

264 Scenes arguably dominated by “sugar” and “gravel” reside in clusters 5 (brown) and
 265 3 (maroon). These patterns should, in the terminology from section 3.2, be understood as
 266 small-scale with rather small voids (or disaggregated/unclustered); “gravel” distinguishes
 267 itself through its higher cloud-top height variance and low directional alignment (see also
 268 left side of fig. 3 b). Cluster 1 (navy) comprises i.a. “fish”, which shares gravel’s void size,
 269 cloud-top height variance and low degree of directional alignment, only at larger scales.
 270 Finally, one may see “flowers” in cluster 7 (blue), as large-scale, aggregated structures with
 271 little directional alignment and low cloud-top height variance.

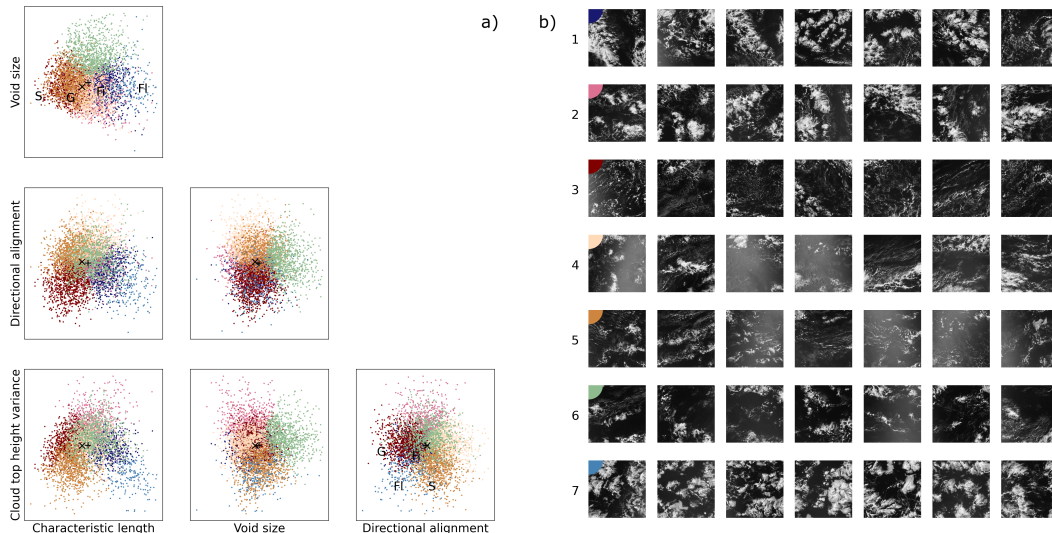


Figure 4. Seven regimes of the 4D pattern description, identified as k-means clusters of different colour: a) Scenes scattered over planes defined by the first four PCs, each normalised to unit variance, named using the convention from section 3.2; b) seven examples of scenes in each regime. Pluses and crosses indicate the distribution’s mean and mode, respectively. S, G, Fi and Fl suggest typical locations for the “sugar”, “gravel”, “fish” and “flowers” patterns diagnosed by Stevens et al. (2019), in the two planes shown in fig. 3, determined by eye.

272 The natural emergence of these regimes from our systematic metric analysis is encour-
 273 agingly consistent with human pattern identification (Stevens et al., 2019) and solidifies
 274 Bony et al. (2020)’s conclusion that these patterns can be objectively identified. However,
 275 even in an unrealistic scenario where all scenes in these four regimes could unambiguously
 276 be labelled sugar, gravel, fish or flowers, they would contain only 52% of the observations in
 277 our dataset. Figure 4 indicates several other regimes that differ in important regards. For
 278 instance, many scenes possess vast voids (cluster 6, sea green). In this regime, clouds likely
 279 affect the region’s climate much less than sugar, gravel, fish or flowers, which all have higher
 280 cloud cover. Analyses of the patterns’ climate sensitivity must probably consider this and
 281 other different regimes explicitly.

282 In fact, pattern classification is itself an approximation. The pattern distribution is *uni-*
 283 *modal* and *continuous* (fig. 2), and therefore does not inherently possess multiple “classes”,
 284 “clusters” or “modes”. Breaking the continuum into clusters neglects subtly different pat-
 285 terns within a cluster. For instance, the band-like sub-regime at high directional alignment
 286 in fig. 3 b) falls within cluster 4 (peach) in fig. 4, even if this sub-regime is visually distinct
 287 from all displayed scenes in cluster 4. To capture such subtleties, we recommend shifting
 288 focus from regimes, classes or clusters of patterns to a more fitting, continuous representa-
 289 tion.

290 Finally, many of the human-identified patterns (sugar, flowers) appear on our distribu-
 291 tion’s extremes (see also fig. 3 a) and b)). While this may explain why they are most
 292 easily distinguished by humans, they lie far from the distribution’s statistical mean and
 293 mode (indicated by pluses and crosses respectively in fig. 4 a) and are thus not typical.
 294 Instead, the modal pattern is partial to smaller scales and voids, which characterise scenes
 295 with shallow, cold-pool dominated convection (clusters 3, 5) or processes on a wide range
 296 of scales (cluster 4); this space may be most relevant to the climatology of patterns.

4 Conclusion and outlook

Research on the climate feedback of patterns in shallow trade-wind cloud fields requires a consistently understood description of those patterns. In this paper, we have systematically developed such a description for square, 500 km² satellite-observed cloud fields east of Barbados. By projecting one new and 20 previously developed organisation metrics onto a set of PCs, we show that cloud patterns can be effectively described as a 4-dimensional, linear combination of *characteristic length*, *void size*, *directional alignment* and *cloud-top height variance*. This description is objective and interpretable, in contrast to direct unsupervised machine learning (objective, not usually interpretable) or human pattern identification (interpretable, not objective). It also demonstrates that patterns follow a continuous, unimodal distribution without distinct classes and that visually striking patterns are extreme, rather than typical. Future studies of the physics behind and climate impact of shallow cloud field patterns can therefore rely either on our PCs or, if accuracy is less important, on metrics that correlate closely to them.

The effectiveness of our approach may well extend to descriptions of deep convective organisation. Many relationships between our metrics are consistent with those found for deep convective cloud fields (Rempel et al., 2017; Brueck et al., 2020), suggesting that an effective, low-dimensional description of deep convective organisation is attainable. Our pattern description could also be used for forecast verification (Jolliffe & Stephenson, 2012), using the pattern distribution’s dimensions as matching criteria between model and observation in similar fashion to e.g. the criteria developed by Wernli et al. (2008). In turn, the forecast verification community may offer useful insights to descriptions of cloud field patterns.

Finally, our approach can itself be refined in several regards. First, using predefined metrics to describe patterns leaves potentially undiscovered information from the description. Therefore, it may be fruitful to compare our approach to more unsupervised machine learning (e.g. Denby, 2020). However, the completeness of a pattern description should ideally be assessed in terms of how fully the underlying processes are separated. This requires process-resolving numerical simulations and/or temporally evolving observations, which link the evolution of the pattern continuum to that of the atmospheric state. Next, our conclusions are tied to our observation scales (1-500 km), meaning that we may inadequately capture this scale window’s extremes. Furthermore, we treat this scale window in an integral sense and ignore patterns that appear on one scale, but may be cancelled by another (Nair et al., 1998). Hence, a further refinement could be to consider pattern distributions on a per-scale basis. Lastly, some subjectivity will likely remain in how different researchers interpret “organisation”. This attests the richness of the underlying patterns, which we hope remains appreciated.

Acknowledgments

MJ and FG acknowledge support by The Branco Weiss Fellowship - Society in Science, administered by ETH Zürich; FG also acknowledges a Veni grant from the Dutch Research Council (NWO). A.P.S acknowledges funding by the European Union’s Horizon 2020 research and innovation programme under grant agreement no. 820829 (CONSTRAIN project). The Aqua and Terra MODIS Clouds 5-Min L2 Swath 1km products, which contain the cloud mask, cloud water path and cloud-top height products used in this study, were extracted from NASA’s Level-1 and Atmosphere Archive & Distribution System (LAADS) Distributed Active Archive Center (DAAC) (http://dx.doi.org/10.5067/MODIS/MYD06_L2.061; http://dx.doi.org/10.5067/MODIS/MOD06_L2.061). All download, preprocessing, metric computation and analysis was done using Python and its Numpy (van der Walt et al., 2011), Pandas (McKinney, 2010) and Scipy (Virtanen et al., 2020) libraries. Field processing and segmentation is done with Scikit Image (van der Walt et al., 2014), PCA and clustering with Scikit Learn (Pedregosa et al., 2011), sparse PCA with Ristretto (Erichson et al., 2020) and plots with Matplotlib (Hunter, 2007) and Seaborn (Waskom & the seaborn de-

349 velopment team, 2020). The integrated code, along with detailed instructions on how to
 350 run it, are available in a living GitHub repository ([https://github.com/martinjanssens/
 351 cloudmetrics](https://github.com/martinjanssens/cloudmetrics)) and its frozen image at the time of submission ([https://doi.org/10.6084/
 352 m9.figshare.12687302.v1](https://doi.org/10.6084/m9.figshare.12687302.v1)).

353 References

- 354 Abdi, H., & Williams, L. J. (2010). Principal component analysis. *Wiley interdisciplinary
 355 reviews: computational statistics*, 2(4), 433–459.
- 356 Benner, T. C., & Curry, J. A. (1998). Characteristics of small tropical cumulus clouds
 357 and their impact on the environment. *Journal of Geophysical Research: Atmospheres*,
 358 103(D22), 28753–28767.
- 359 Bony, S., & Dufresne, J.-L. (2005). Marine boundary layer clouds at the heart of tropical
 360 cloud feedback uncertainties in climate models. *Geophysical Research Letters*, 32(20).
- 361 Bony, S., Schulz, H., Vial, J., & Stevens, B. (2020). Sugar, gravel, fish and flowers: De-
 362 pendence of mesoscale patterns of trade-wind clouds on environmental conditions.
 363 *Geophysical Research Letters*.
- 364 Bretherton, C. (2015). Insights into low-latitude cloud feedbacks from high-resolution
 365 models. *Philosophical Transactions of the Royal Society A: Mathematical, Physical
 366 and Engineering Sciences*, 373(2054), 20140415.
- 367 Bretherton, C., & Blossey, P. (2017). Understanding mesoscale aggregation of shallow
 368 cumulus convection using large-eddy simulation. *Journal of Advances in Modeling
 369 Earth Systems*, 9(8), 2798–2821.
- 370 Brueck, M., Hohenegger, C., & Stevens, B. (2020). Mesoscale marine tropical precipitation
 371 varies independently from the spatial arrangement of its convective cells. *Quarterly
 372 Journal of the Royal Meteorological Society*, 146(728), 1391–1402.
- 373 Brune, S., Kapp, F., & Friederichs, P. (2018). A wavelet-based analysis of convective organ-
 374 ization in ICON large-eddy simulations. *Quarterly Journal of the Royal Meteorological
 375 Society*, 144(717), 2812–2829.
- 376 Cadima, J., & Jolliffe, I. T. (1995). Loading and correlations in the interpretation of
 377 principle compenents. *Journal of applied Statistics*, 22(2), 203–214.
- 378 Cahalan, R. F., & Joseph, J. H. (1989). Fractal statistics of cloud fields. *Monthly weather
 379 review*, 117(2), 261–272.
- 380 Denby, L. (2020). Discovering the importance of mesoscale cloud organization through
 381 unsupervised classification. *Geophysical Research Letters*, 47(1), e2019GL085190.
- 382 de Roode, S. R., Duynkerke, P. G., & Jonker, H. J. (2004). Large-eddy simulation: How
 383 large is large enough? *Journal of the atmospheric sciences*, 61(4), 403–421.
- 384 Erichson, N. B., Zheng, P., Manohar, K., Brunton, S. L., Kutz, J. N., & Aravkin, A. Y.
 385 (2020). Sparse principal component analysis via variable projection. *SIAM Journal
 386 on Applied Mathematics*, 80(2), 977–1002.
- 387 Glassmeier, F., & Feingold, G. (2017). Network approach to patterns in stratocumulus
 388 clouds. *Proceedings of the National Academy of Sciences*, 114(40), 10578–10583.
- 389 Holloway, C. E., Wing, A. A., Bony, S., Muller, C., Masunaga, H., L’Ecuyer, T. S., ...
 390 Zuidema, P. (2017). Observing convective aggregation. *Surveys in Geophysics*, 38(6),
 391 1199–1236.
- 392 Hunter, J. D. (2007). Matplotlib: A 2d graphics environment. *Computing in Science &
 393 Engineering*, 9(3), 90–95. doi: 10.1109/MCSE.2007.55
- 394 Johnson, R. H., Rickenbach, T. M., Rutledge, S. A., Ciesielski, P. E., & Schubert, W. H.
 395 (1999). Trimodal characteristics of tropical convection. *Journal of climate*, 12(8),
 396 2397–2418.
- 397 Jolliffe, I. T., & Stephenson, D. B. (2012). *Forecast verification: a practitioner’s guide in
 398 atmospheric science*. John Wiley & Sons.
- 399 Jonker, H. J., Duynkerke, P. G., & Cuijpers, J. W. (1999). Mesoscale fluctuations in scalars
 400 generated by boundary layer convection. *Journal of the atmospheric sciences*, 56(5),
 401 801–808.

- 402 Klein, S. A., Hall, A., Norris, J. R., & Pincus, R. (2017). Low-cloud feedbacks from cloud-
 403 controlling factors: a review. In *Shallow clouds, water vapor, circulation, and climate*
 404 *sensitivity* (pp. 135–157). Springer.
- 405 McKinney, W. (2010). Data Structures for Statistical Computing in Python. In Stéfan
 406 van der Walt & Jarrod Millman (Eds.), *Proceedings of the 9th Python in Science*
 407 *Conference* (p. 56 - 61). doi: 10.25080/Majora-92bf1922-00a
- 408 Medeiros, B., & Nuijens, L. (2016). Clouds at Barbados are representative of clouds across
 409 the trade wind regions in observations and climate models. *Proceedings of the National*
 410 *Academy of Sciences*, *113*(22), E3062–E3070.
- 411 Muller, C. J., & Held, I. M. (2012). Detailed investigation of the self-aggregation of con-
 412 vection in cloud-resolving simulations. *Journal of the Atmospheric Sciences*, *69*(8),
 413 2551–2565.
- 414 Nair, U., Weger, R., Kuo, K., & Welch, R. (1998). Clustering, randomness, and regularity
 415 in cloud fields: 5. the nature of regular cumulus cloud fields. *Journal of Geophysical*
 416 *Research: Atmospheres*, *103*(D10), 11363–11380.
- 417 Neggers, R., Griewank, P., & Heus, T. (2019). Power-law scaling in the internal variability of
 418 cumulus cloud size distributions due to subsampling and spatial organization. *Journal*
 419 *of the Atmospheric Sciences*, *76*(6), 1489–1503.
- 420 Nuijens, L., & Siebesma, A. P. (2019). Boundary layer clouds and convection over subtrop-
 421 ical oceans in our current and in a warmer climate. *Current Climate Change Reports*,
 422 *5*(2), 80–94.
- 423 Pedregosa, F., Varoquaux, G., Gramfort, A., Michel, V., Thirion, B., Grisel, O., ... Duch-
 424 esnay, E. (2011). Scikit-learn: Machine learning in Python. *Journal of Machine*
 425 *Learning Research*, *12*, 2825–2830.
- 426 Platnick, S., Ackerman, S., King, M., Menzel, P., Wind, G., & Frey, R. (2015).
 427 *MODIS Atmosphere L2 Cloud Product (06_L2)*. Goddard Space Flight Center, USA:
 428 NASA MODIS Adaptive Processing System. doi: [http://dx.doi.org/10.5067/MODIS/](http://dx.doi.org/10.5067/MODIS/MYD06_L2.061)
 429 [MYD06_L2.061](http://dx.doi.org/10.5067/MODIS/MYD06_L2.061)
- 430 Pscheidt, I., Senf, F., Heinze, R., Deneke, H., Trömel, S., & Hohenegger, C. (2019). How
 431 organized is deep convection over germany? *Quarterly Journal of the Royal Meteorolo-*
 432 *gical Society*, *145*(723), 2366–2384.
- 433 Rasp, S., Selz, T., & Craig, G. C. (2018). Variability and clustering of midlatitude sum-
 434 mertime convection: Testing the Craig and Cohen theory in a convection-permitting
 435 ensemble with stochastic boundary layer perturbations. *Journal of the Atmospheric*
 436 *Sciences*, *75*(2), 691–706.
- 437 Rempel, M., Senf, F., & Deneke, H. (2017). Object-based metrics for forecast verification of
 438 convective development with geostationary satellite data. *Monthly Weather Review*,
 439 *145*(8), 3161–3178.
- 440 Rieck, M., Nuijens, L., & Stevens, B. (2012). Marine boundary layer cloud feedbacks in a
 441 constant relative humidity atmosphere. *Journal of the Atmospheric Sciences*, *69*(8),
 442 2538–2550.
- 443 Schneider, T., Teixeira, J., Bretherton, C. S., Brient, F., Pressel, K. G., Schär, C., &
 444 Siebesma, A. P. (2017). Climate goals and computing the future of clouds. *Nature*
 445 *Climate Change*, *7*(1), 3–5.
- 446 Scott, D. W. (1992). *Multivariate density estimation: theory, practice, and visualization*.
 447 John Wiley & Sons.
- 448 Seifert, A., & Heus, T. (2013). Large-eddy simulation of organized precipitating trade wind
 449 cumulus clouds. *Atmos. Chem. Phys*, *13*(11), 5631–5645.
- 450 Stevens, B., Bony, S., Brogniez, H., Hentgen, L., Hohenegger, C., Kiemle, C., ... others
 451 (2019). Sugar, gravel, fish and flowers: Mesoscale cloud patterns in the trade winds.
 452 *Quarterly Journal of the Royal Meteorological Society*, 1–12.
- 453 Tobin, I., Bony, S., & Roca, R. (2012). Observational evidence for relationships between the
 454 degree of aggregation of deep convection, water vapor, surface fluxes, and radiation.
 455 *Journal of Climate*, *25*(20), 6885–6904.
- 456 Tompkins, A. M., & Semie, A. G. (2017). Organization of tropical convection in low

- 457 vertical wind shears: Role of updraft entrainment. *Journal of Advances in Modeling*
458 *Earth Systems*, 9(2), 1046–1068.
- 459 van der Walt, S., Colbert, S. C., & Varoquaux, G. (2011). The numpy array: a structure for
460 efficient numerical computation. *Computing in Science & Engineering*, 13(2), 22–30.
- 461 van der Walt, S., Schönberger, J. L., Nunez-Iglesias, J., Boulogne, F., Warner, J. D., Yager,
462 N., . . . the scikit-image contributors (2014, 6). scikit-image: image processing in
463 Python. *PeerJ*, 2, e453. Retrieved from <https://doi.org/10.7717/peerj.453> doi:
464 10.7717/peerj.453
- 465 van Laar, T. W. (2019). *Spatial patterns in shallow cumulus cloud populations over a*
466 *heterogeneous surface* (Doctoral dissertation, University of Cologne). Retrieved from
467 <http://kups.ub.uni-koeln.de/id/eprint/10221>
- 468 Virtanen, P., Gommers, R., Oliphant, T. E., Haberland, M., Reddy, T., Cournapeau, D.,
469 . . . Contributors, S. . . (2020). SciPy 1.0: Fundamental Algorithms for Scientific
470 Computing in Python. *Nature Methods*, 17, 261–272. doi: [https://doi.org/10.1038/](https://doi.org/10.1038/s41592-019-0686-2)
471 [s41592-019-0686-2](https://doi.org/10.1038/s41592-019-0686-2)
- 472 Waskom, M., & the seaborn development team. (2020, September). *mwaskom/seaborn*.
473 Zenodo. Retrieved from <https://doi.org/10.5281/zenodo.592845> doi: 10.5281/
474 [zenodo.592845](https://doi.org/10.5281/zenodo.592845)
- 475 Weger, R., Lee, J., Zhu, T., & Welch, R. (1992). Clustering, randomness and regular-
476 ity in cloud fields: 1. theoretical considerations. *Journal of Geophysical Research:*
477 *Atmospheres*, 97(D18), 20519–20536.
- 478 Wernli, H., Paulat, M., Hagen, M., & Frei, C. (2008). SAL — a novel quality measure
479 for the verification of quantitative precipitation forecasts. *Monthly Weather Review*,
480 136(11), 4470–4487.
- 481 White, B., Buchanan, A., Birch, C., Stier, P., & Pearson, K. (2018). Quantifying the effects
482 of horizontal grid length and parameterized convection on the degree of convective
483 organization using a metric of the potential for convective interaction. *Journal of the*
484 *Atmospheric Sciences*, 75(2), 425–450.
- 485 Windmiller, J. M. (2017). *Organization of tropical convection* (Doctoral dissertation,
486 Ludwig-Maximilian University of Munich). Retrieved from [https://edoc.ub.uni-](https://edoc.ub.uni-muenchen.de/21245/)
487 [muenchen.de/21245/](https://edoc.ub.uni-muenchen.de/21245/)
- 488 Wood, R., & Field, P. R. (2011). The distribution of cloud horizontal sizes. *Journal of*
489 *Climate*, 24(18), 4800–4816.
- 490 Wood, R., & Hartmann, D. L. (2006). Spatial variability of liquid water path in marine low
491 cloud: The importance of mesoscale cellular convection. *Journal of Climate*, 19(9),
492 1748–1764.
- 493 Zou, H., Hastie, T., & Tibshirani, R. (2006). Sparse principal component analysis. *Journal*
494 *of computational and graphical statistics*, 15(2), 265–286.